Supplementary information: Bloch oscillations and matter-wave localization of a dipolar quantum gas in a one-dimensional lattice

Gabriele Natale,[1,2] Thomas Bland,[2] Simon Gschwendtner,[2] Louis Lafforgue,[2]
Daniel S. Grün,[2] Alexander Patscheider,[2] Manfred J. Mark,[1,2] and Francesca Ferlaino[1,2]
[1] *Institut für Quantenoptik und Quanteninformation, Österreichische Akademie der Wissenschaften, Technikerstraße 21a, 6020 Innsbruck, Austria*
[2] *Institut für Experimentalphysik, Universität Innsbruck, Technikerstraße 25, 6020 Innsbruck, Austria*

SUPPLEMENTARY NOTE 1: ENERGY CONTRIBUTION

The rich phase diagram of dipolar atoms relies on the competition between the different interaction terms. In Fig. S1 we assess the different interaction energy contributions to Eq. (6) for a range of scattering lengths. For $a_\mathrm{s} > a_\mathrm{dd}$ the total interaction energy is positive, and it corresponds to a dilute BEC. Following a_s to smaller values all interaction contributions are almost constant, until at around $a_\mathrm{s} = 60\,a_0$ there is a phase transition from the BEC to droplet state, as identified in Fig. 4 of the main text. This sharp gradient ceases at around $a_\mathrm{s} = 55\,a_0$, where the atoms are localized to a single lattice plane. Note that although the DDI offsite energy is typically only 10% of the onsite counterpart, it constitutes a significant contribution to the total interaction energy in the system, shifting the BEC to droplet crossover and localization transitions by a few a_0.

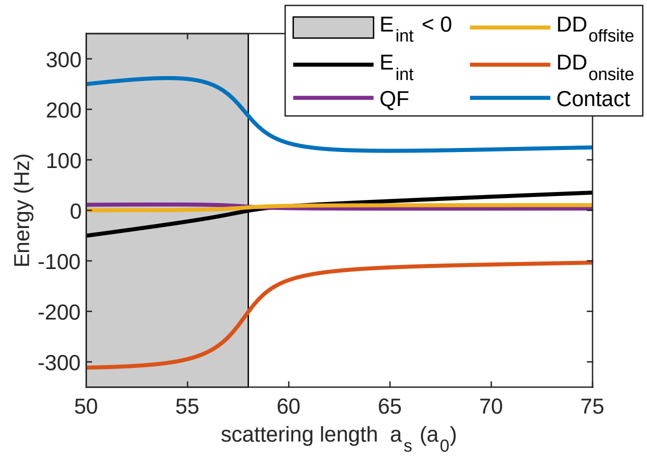

FIG. S1. **Interaction energy contributions.** Scattering length dependency of the individual interaction contributions of the ground state solutions from the 1D model, calculated for $N = 10^4$ atoms.

SUPPLEMENTARY NOTE 2: 2D TO 3D CROSSOVER

The dimensionality of the system is known to highly influence the size and even the sign of the beyond-mean-field contribution, in both Bose-Bose[1–3] and dipolar[4–6] gases. Here, we assess the validity of employing the full 3D LHY correction to our system. Following Ref.,[6] we define the dimensionless parameter $\xi = gn/\epsilon_0$–dependent on the contact interactions g, peak 3D density n, and the confinement energy scale $\epsilon_0 = \hbar^2\pi^2/2mz_\mathrm{ho}^2$–that indicates which dimensionality regime our system is in. If $\xi \gtrsim 1$ we are safe to use the 3D LHY term, whereas if $\xi \ll 1$ the 2D solution deviates from the 3D one. Deep in the localized droplet regime, where the peak density is on the order of $10^{22}\mathrm{m}^{-3}$, we find $\xi \approx 2$, and the 3D LHY as used throughout this work is valid. Even at large scattering lengths, where the peak density is closer to $5\times10^{20}\mathrm{m}^{-3}$, we find $\xi \approx 0.5$, which introduces an error of less than 5% between the 2D and 3D LHY terms.[6] In this limit, the 2D LHY term may be more appropriate, however in the dilute BEC phase the impact of the LHY is minimal.

SUPPLEMENTARY NOTE 3: ANALYTIC MODEL OF DEPHASING

Starting from the discrete 1D eGPE we decompose the coefficients c_j into amplitude and phase as $c_j = |c_j|\exp(-i\phi_j)$, and then integrate Eq. (4) in time to give

$$\begin{aligned}\phi_j(t) = \Bigg(-F_\mathrm{ext}z_j + g^\mathrm{1D}N|c_j|^2 + N\sum_k U^\mathrm{dd}_{|j-k|}|c_k|^2 \\ + \gamma^\mathrm{1D}_\mathrm{QF}N^{3/2}\gamma_\mathrm{QF}|c_j|^3\Bigg)\frac{t}{\hbar} \\ \equiv \left(-F_\mathrm{ext}z_j + \mu_j\right)\frac{t}{\hbar}\,, \qquad \text{(S1)}\end{aligned}$$

with onsite chemical potentials μ_j, and where we have also assumed that $F_\mathrm{ext}d \gg J$ such that the amplitudes $|c_j|$ are frozen.

Following Ref.,[7] we write the Fourier transform of the quasi-1D wavefunction as

$$\psi(k,t) = w(k)\sum_j |c_j|\exp[-i(kz_j + \phi_j(t))] = w(k)\tilde{C}(k,t)\,, \qquad \text{(S2)}$$

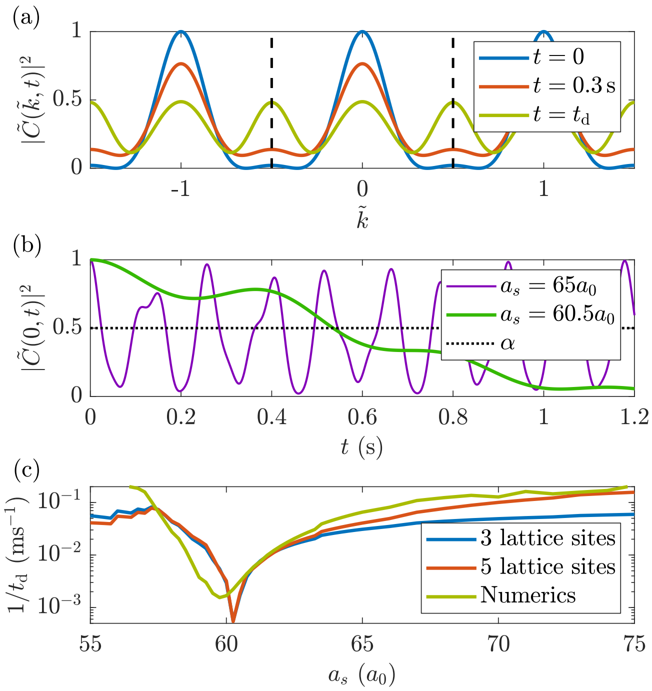

FIG. S2. **Analytic dephasing rate.** **(a)** Evolution of the function $\tilde{C}$, with $\tilde{k}$ normalized to the Brillouin zone in the moving frame, and $a_\mathrm{s} = 60.5\,a_0$. Here, the solution of Eq. (S4) is $t_\mathrm{d} = 0.59$s. **(b)** Time evolution of the central point of $\tilde{C}$, showing when $|\tilde{C}|^2$ crosses $\alpha = 0.5$. The function $\tilde{C}$ is scaled to the value at $\tilde{C}(0,0)$. **(c)** Analytic dephasing rate ($\gamma = 1/t_\mathrm{d}$) obtained for the 3 lattice site approximation Eq. (S4) and the 5 lattice site approximation Eq. (S5), compared to the numerically obtained value from a real-time simulation of the discrete model, Eq. (4).

where $w(k)$ is the momentum space Wannier function, and phases ϕ_j are given above. If all interactions are set to zero this function is initially a delta function situated at $k = 0$ and moves in k-space as $\tilde{k} = k - F_\mathrm{ext}t/\hbar$. Interactions broaden $\tilde{C}(k,t)$, leading to a dephasing of coefficients c_j. Fig. S2(a) depicts $|\tilde{C}(k,t)|^2$ as a function of k at different times t, normalized to $|\tilde{C}(0,0)|^2$.

We extract an analytic approximation to the dephasing time by considering the temporal behaviour of the point $|\tilde{C}(0,t)|^2$, i.e. at $\tilde{k} = 0$. During dephasing this point rapidly decreases through interference between neighboring sites. This quantity is plotted in Fig. S2(b) for a few example scattering lengths. It reaches the threshold $\alpha/\tilde{C}(0,0) = 0.5$ at the dephasing time $t = t_\mathrm{d}$, where many k-modes are now highly occupied. This time can be found through the smallest positive solution of

$$\alpha = \left| \left(\sum_j |c_j| \cos\left(\frac{\mu_j t_\mathrm{d}}{\hbar}\right)\right)^2 + \left(\sum_j |c_j| \sin\left(\frac{\mu_j t_\mathrm{d}}{\hbar}\right)\right)^2 \right| . \tag{S3}$$

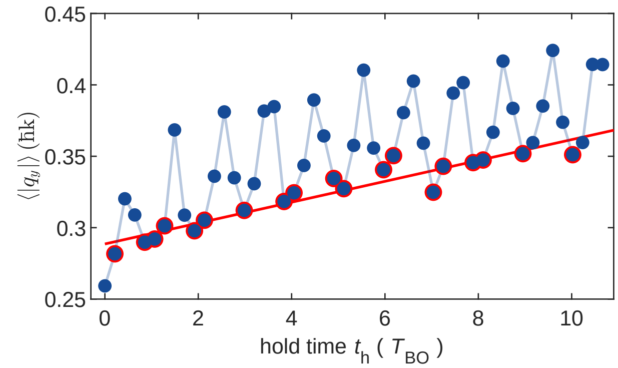

FIG. S3. **Evolution of the** $\langle|q_z|\rangle$**.** In the figure $\langle|q_z|\rangle$ as a function of time for a_s=58.8 a_0. The points with red edges are the one selected for the fit. The red line corresponds to the fit result $A(t-\tau)+0.5$

Exact solutions to $|\tilde{C}(0,t_\mathrm{d})|^2 = \alpha$ can be only found in limiting cases. For the three lattice site case, with $j = -1, 0, 1$ and noting the symmetry of $|c_j| = |c_{-j}|$ we obtain

$$t_\mathrm{d} = \left| \arccos\left(\frac{4|c_0c_1|}{\alpha + |c_0|^2 - 2}\right) \frac{\hbar}{(\mu_1 - \mu_0)} \right| , \tag{S4}$$

This relation is expected to give an accurate prediction of the dephasing time for all states where only 3 lattice sites are dominant. From this equation, one can see how the dephasing time tends to infinity in the limit of equally distributed chemical potentials, as observed in Fig. 2 of the main text. We can extend this to 5 sites, but it is not as trivial. One needs to numerically solve the transcendental equation

$$\begin{aligned}\alpha =& \Bigg| 2 - |c_0|^2 + 4|c_0c_1| \cos\left(\frac{(\mu_0-\mu_1)t_\mathrm{d}}{\hbar}\right) \\ &+ 4|c_0c_2| \cos\left(\frac{(\mu_0-\mu_2)t_\mathrm{d}}{\hbar}\right) \\ &+ 8|c_1c_2| \cos\left(\frac{(\mu_1-\mu_2)t_\mathrm{d}}{\hbar}\right) \Bigg| ,\end{aligned} \tag{S5}$$

for the smallest non-zero root t_d. We compare the results from Eqs. (S4) and (S5) to the numerically obtained dephasing rate, $\gamma = 1/t_\mathrm{d}$, in Fig. S2(c), as presented in Fig. 2 of the main text, and find excellent agreement.

SUPPLEMENTARY NOTE 4: ANALYSIS OF MOMENTUM DISTRIBUTION DURING BLOCH OSCILLATION

When the Bloch oscillation dephases, the width of the momentum distribution increases with time.[8] To evaluate the dephasing rate we analyze the 1D momentum distribution along z, $n(q_z)$, as a function of the holding time. Because of our limited vertical optical access, the

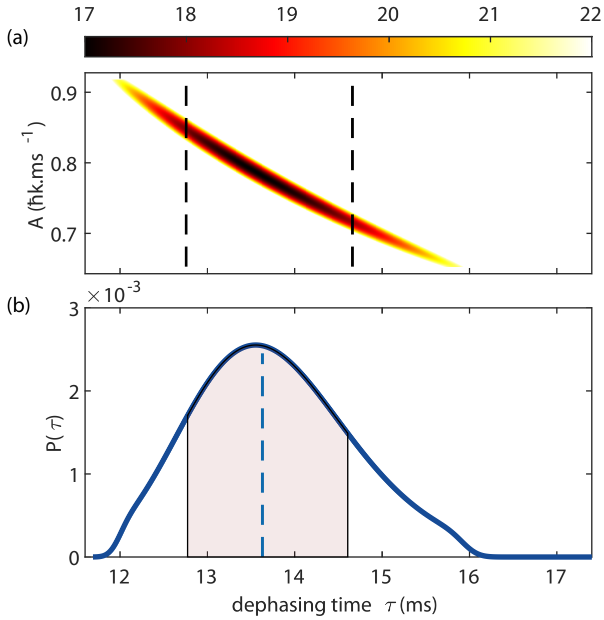

FIG. S4. **Uncertainties χ^2 analysis**. **(a)** χ^2 as a function of A and τ. The black dash lines correspond to the value $\chi^2_{min}+1$. Below, **(b)** probability distribution of τ, given by numerical integration of $\int_A dAe^{-\chi^2(A,\tau)/2}$ and normalization to 1. a_s=58.8 a_0. The dashed line indicates the fit result and the shaded area the 68% confidence interval.

1D lattice is not perfectly aligned with the z (gravity) direction. We measure a tilt of 9(1)°. Such a tilt effectively weakens the radial trapping strength, limiting our observation time to 12 ms, which anyhow allows us to observe up to 25 BO period.

From $n(q_z)$, we can extract the maximum position ($q_z^{\max}$) and the quantity $\langle|q_z|\rangle$, given by

$$\langle|q_z|\rangle = \sum_{q_z} n(q_z)\,|q_z - q_z^{\max}|\,.$$

This quantity is proportional to the width of the distribution. In Fig. S3, we report $\langle|q_z|\rangle$ for a_s= 65.7(1.0) a_0. To quantify the dephasing rate γ, we apply a linear fit to $\langle|q_z|\rangle$. For the fit, we select only the points at the center of the Brillouin zone, up to the time when $\langle|q_z|\rangle$ is reaching the fully dephased configuration, $0.5\hbar k$. Indeed, when the cloud is at the edge of the Brillouin zone, $\langle|q_z|\rangle$ is artificially increased and it does not represent the dephasing, as shown in Fig. S3. We define the dephasing rate γ as the inverse of the time τ that the fitted function needs to reach the value $0.5\,\hbar k$. Thus, using the fit parametrization $A(t-\tau)+0.5$, where A and τ are the fitting variables and t is the time, we can directly extract τ and its inverse γ.

To determine the uncertainties with our non-linear parametrization, we analyze the $\chi^2(A,\tau)$. We estimate the uncertainties on our data points by assuming equal statistical fluctuations around our fitting model and using the expected value $\langle\chi^2\rangle = N_\mathrm{data}-2$. Figure S4 shows a clear asymmetric shape for χ^2, indicating asymmetric uncertainties on our fit parameters. As we are only interested in the uncertainties on τ, we consider $P_{\chi^2}(\tau) = \frac{1}{N}\int_A dAe^{-\chi^2(A,\tau)/2}$, with N a normalization constant. $P_{\chi^2}(\tau)$ corresponds to the probability distribution of τ for our fitting model. Finally, from $P_{\chi^2}(\tau)$, we define the 68% confident interval of our dephasing rate γ shown in Fig. S4.

In order to compare our experimental data with the theoretical predictions, we repeat the same analysis with the data from the 1D discrete model. Since in the experiment the condensed atom number changes with the scattering length, see Fig. 4, the atom number considered in the theoretical simulations varies accordingly. In Fig. 2, we account for the experimental fluctuations by taking an interval of ±20% of the BEC atoms number. For each scattering length, we determine the extreme values of γ in the ±20% range, which we use to create the shaded area.

1. Petrov, D. S. & Astrakharchik, G. E. Ultradilute low-dimensional liquids. *Phys. Rev. Lett.* **117**, 100401 (2016).
2. Ilg, T., Kumlin, J., Santos, L., Petrov, D. S. & Büchler, H. P. Dimensional crossover for the beyond-mean-field correction in bose gases. *Physical Review A* **98**, 051604 (2018).
3. Lavoine, L. & Bourdel, T. Beyond-mean-field crossover from one dimension to three dimensions in quantum droplets of binary mixtures. *Phys. Rev. A* **103**, 033312 (2021).
4. Edler, D. *et al.* Quantum fluctuations in quasi-one-dimensional dipolar bose-einstein condensates. *Phys. Rev. Lett.* **119**, 050403 (2017).
5. Boudjemâa, A. Two-dimensional quantum droplets in dipolar bose gases. *New Journal of Physics* **21**, 093027 (2019).
6. Zin, P., Pylak, M., Wasak, T., Jachymski, K. & Idziaszek, Z. Quantum droplets in a dipolar bose gas at a dimensional crossover. *Journal of Physics B: Atomic, Molecular and Optical Physics* **54**, 165302 (2021).
7. Witthaut, D., Werder, M., Mossmann, S. & Korsch, H. J. Bloch oscillations of bose-einstein condensates: Breakdown and revival. *Phys. Rev. E* **71**, 036625 (2005).
8. Morsch, O., Müller, J. H., Cristiani, M., Ciampini, D. & Arimondo, E. Bloch oscillations and mean-field effects of bose-einstein condensates in 1d optical lattices. *Phys. Rev. Lett.* **87**, 140402 (2001).